Solid State Sciences 51 (2016) 24–29

Contents lists available at ScienceDirect

Solid State Sciences

journal homepage: www.elsevier.com/locate/ssscie

Synthesis and photocatalytic properties of vertically aligned Bi_2S_3 platelets

Chunjuan Tang [a, *], Yongsheng Zhang [a], Jianfeng Su [a], Changqing Wang [a], Ruirui Sun [a], Jiao Zhang [a], Guanghai Li [b]

[a] Department of Mathematics and Physics, Luoyang Institute of Science and Technology, Luoyang 471023, PR China
[b] Key Laboratory of Materials Physics, Anhui Key Laboratory of Nanomaterials and Nanotechnology, Institute of Solid State Physics, Chinese Academy of Sciences, Hefei 230031, PR China

ARTICLE INFO

Article history:
Received 22 December 2014
Received in revised form
30 October 2015
Accepted 10 November 2015
Available online 14 November 2015

Keywords:
Bi_2S_3
Platelet
FTO
Photocatalytic

ABSTRACT

Vertically aligned Bi_2S_3 platelets have been synthesized on FTO substrate *via* a simple hydrothermal process. X-ray diffraction analysis confirms the orthorhombic structure of the platelets. The results of scanning electron microscopy show that the Bi_2S_3 platelets interconnect with each other. The length of platelets is about 5 μm and the thickness ranges from 50 to 150 nm. The photocatalytic activity studies reveal that the synthesized Bi_2S_3 platelets exhibit excellent photocatalytic performance in rapidly degrading aqueous methylene blue dye solution under UV irradiation. A degradation ratio of 56% was obtained for the Bi_2S_3 platelets at 120 min and about 99% at 240 min. These results suggest that Bi_2S_3 platelets will be an interesting candidate for photocatalytic detoxification under UV light.

© 2015 Elsevier Masson SAS. All rights reserved.

1. Introduction

The energy crisis and environmental pollution are the two major problems for our society and threaten our lives quality seriously. For the purpose of water purification and release hydrogen from water for clean energy generation, photocatalysts have received considerable attention because of their ability to decompose organic compounds into inorganic ones [1–3]. Most photocatalysts have been synthesized based on metal oxides, such as TiO_2 and ZnO [4–7]. In recent years, it is reported that some metal sulfides show high efficiency in photodegradation [8–12], which indicates that metal sulfides can also be used as phtocatalysts. Bi_2S_3, a direct band gap semiconductor, has been widely used in many fields, such as photovoltaic material and sensors [13–16]. Now it has attracted much attention as a novel photocatalyst [17–20].

The photocatalyst used to be nanopowders. However, when the photocatalyst powder is suspended into liquid phase, the problems exist since it is difficult to separate the fine particles and recycle. When immobilizing the semiconductor catalyst film on the solid support, it is easy to separate and recycle, but it will obviously decrease the contact area between the photocatalyst and solution. To increase the contact area between the photocatalyst and solution, some groups immobilize two-dimensional (2D) nanostructures on solid support. Wang et al. reported that TiO_2 nanosheet arrays exhibited superior photocatalytic efficiency under UV illumination as compared with the relevant commercial products P25 [21]. Mu et al. reported that BiOCl nanosheet arrays obtained *via* hydrothermal method exhibited excellent activity and retained much better photocatalytic stability in durability tests [22].

Up to now, there have been a few reports on the fabrication of Bi_2S_3 2D nanostructures [23–28], but the photocatalytic properties of this kind of nanostructure have been scarcely reported. Recently, direct growth of nanostructured thin films on FTO or bare glass substrates under hydrothermal conditions have been successfully realized for large quantities of sulfide [29,30]. In this work, vertically aligned Bi_2S_3 platelets on FTO substrate were synthesized *via* simple hydrothermal approach. The effects of the temperature and reaction time on the growth of the vertically aligned Bi_2S_3 platelets have been investigated. Photocatalytic activities in the degradation of methylene blue (MB) are also studied and the prepared platelets are found to have high photodegradation efficiency. The new photocatalyst has potential applications in environmental remediation.

* Corresponding author.
E-mail address: tangchunjuan@163.com (C. Tang).

http://dx.doi.org/10.1016/j.solidstatesciences.2015.11.004
1293-2558/© 2015 Elsevier Masson SAS. All rights reserved.

2. Experimental

All of the chemical reagents are of analytical grade and used without further purification. The transparent conductive fluorine-doped tin oxide (FTO) glass substrate was ultrasonically cleaned sequentially in acetone, alcohol, and distilled water for 10 min (min) each and was finally dried in air. In a typical preparing process, 0.61 g $Bi(NO)_3 \cdot 5H_2O$ was dissolved into 60 mL distilled water, then 0.25 g thiourea (Tu) was added into the above solution. The solution became yellow immediately, indicating the formation of Bi–Tu complex. After being stirred for 10 min, the yellow solution was transferred to a Teflon-lined stainless-steel autoclave with a capacity of 100 mL, in which the well-cleaned FTO substrate was placed at the bottom of the Teflon liner with the conductive side facing up. The Teflon liner was sealed in an autoclave and maintained at 160 °C for 8 h (h). After that, the autoclave was cooled to room temperature naturally. The FTO substrate was taken out, rinsed extensively with distilled water and dried in ambient air at 60 °C.

The purity and composition of the as-prepared sample was examined with X-ray powder diffraction (XRD, Philips X'pert PRO with Cu–K line radiation). The morphology and microstructure were characterized with field-emission scanning electron microscopy (SEM, FEI Sirion-200), transmission electron microscopy (TEM, JEM-2010), and high-resolution transmission electron microscope (HRTEM, JEOL 2010) associated with selected-area electron diffraction (SAED).

The photocatalytic experiments were performed in a Pyrex photoreactor. The FTO substrate covered with Bi_2S_3 platelets was affixed to the inside wall of the photoreactor with the conductive side facing toward the UV lamp. The photoreactor was filled with MB solution (1×10^{-5} M, 300 ml) to submerge the substrate. A 125 W UV lamp with a maximum emission at about 365 nm was used to irradiate the reaction system. After different irradiation intervals, analytical samples for absorption measurement were taken out for measurement by UV–vis spectrophotometer.

3. Results and discussion

Fig. 1a shows the typical XRD pattern of the resulting Bi_2S_3 platelets on the substrate. All the diffraction peaks can be indexed as the orthorhombic structured Bi_2S_3 (JCPDS NO. 75-1306, $a = 1.111$ nm, $b = 1.125$ nm and $c = 0.397$ nm). The intense and sharp diffraction peaks suggest that the as-prepared product has a high crystallinity. No other diffraction peaks of impurity phase were observed, indicating a good purity and completed reaction during the process. Nitrogen adsorption–desorption shown in Fig. 1b displays a type IV isotherm with a distinct hysteresis loop. The Brurauer–Emmerr–Teller (BET) surface area of the product is determined to be 23.01 m^2/g, which is higher than that of Bi_2S_3 rods (11.41 m^2/g).

Fig. 2a shows the representative SEM image of vertically aligned Bi_2S_3 platelets on the FTO substrate grown at 160 °C for 8 h. It can be seen that the film exhibits a porous architecture, which consists of interconnected platelets with a length of about 5 μm. The magnified image (Fig. 2b) shows that the platelets grow almost perpendicularly on the substrate and the thickness of the platelets ranges from 50 to 150 nm. The gap between the platelets was about 500–1500 nm, which indicates that the film has a potentially large surface area.

The obtained product was further investigated by TEM, as shown in Fig. 2c. It also demonstrates the formation of platelets, matching well with the typical morphology of the building blocks in the film. HRTEM shown in Fig. 2d was carried out for more detailed structural information. Clear lattice fringes can be observed and the single-crystalline nature of the platelet is revealed. The lattice spacing of about 0.311 nm corresponds to the distance between adjacent (211) planes, while the lattice spacing of 0.355 nm corresponds to the distance between adjacent (130) planes. The angle between (211) and (130) planes in Fig. 2d is 64°, which is consistent with the calculated value of 63.88°. The inset in Fig. 2d is the corresponding SAED images of the platelet, which also indicates that the platelet is single-crystalline.

To investigate the growth process of Bi_2S_3 platelets on the substrate, time-dependent experiments were carried out, in which samples were collected at different reaction time while keeping other experimental conditions the same. A series of interesting morphological evolutions of products were obtained. It can be seen clearly that FTO conductive substrate was covered by block-shaped particles (Fig. 3a). In the early stages, the FTO particles might act as seed crystals for the growth of Bi_2S_3. As soon as the reaction began, Bi_2S_3 nucleated on the FTO particles. After hydrothermal for 30 min, a dark-grey sparse precipitate with irregular particle shape was formed on the substrate (Fig. 3b). With a prolonged reaction time of 90 min, the nuclei rapidly developed into many regimental petals based on their layered graphene-like structure (Fig. 3c). The

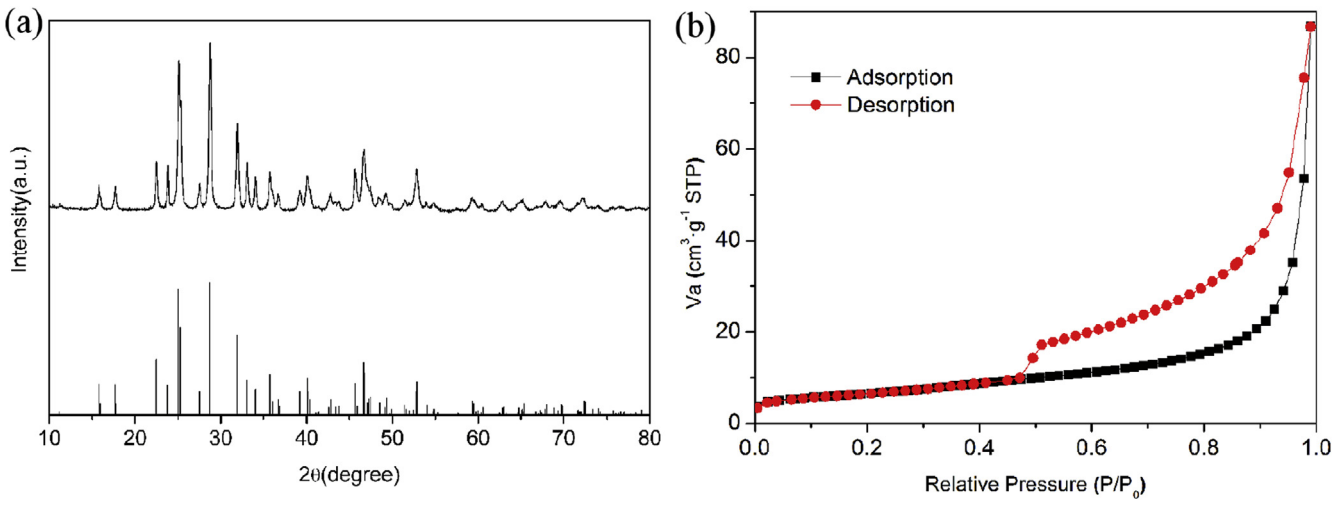

Fig. 1. (a) XRD pattern and (b) Nitrogen adsorption–desorption isotherm of vertically aligned Bi_2S_3 platelets.

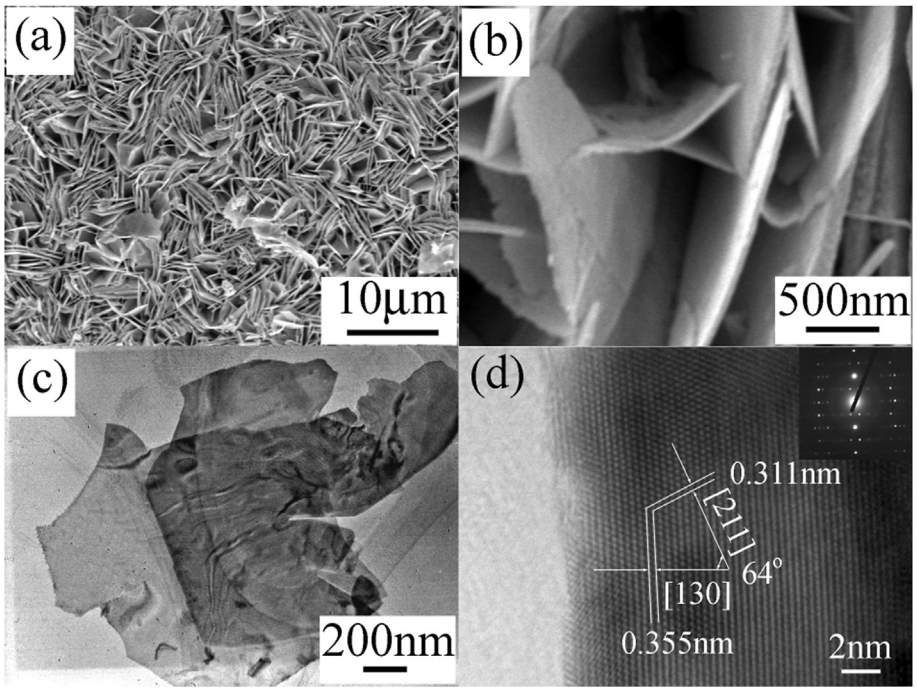

Fig. 2. (a) low and (b) high magnification SEM images of vertically aligned Bi_2S_3 platelets, (c) TEM image of the Bi_2S_3 platelet, (d) HRTEM image of the platelet, the inset is the corresponding SAED.

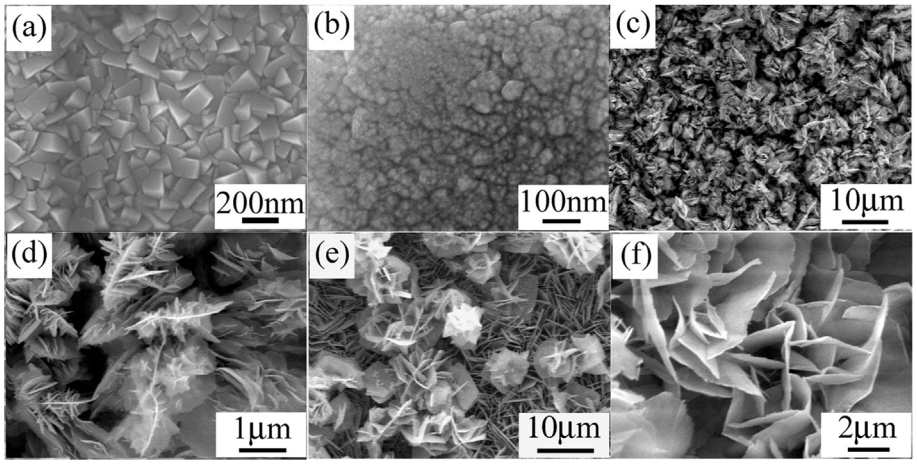

Fig. 3. (a) SEM image of FTO surface, SEM images of the as-products: (b) 30 min, (c) and (d) 90 min, (e) and (f) 12 h.

regimental petals were composed of several thin slices, which can be seen clearly in the magnified image (Fig. 3d). With the reaction proceeding, the thin slices developed to grow into platelet. When the reaction time was 8 h, the growing platelet touched each other and evolved into a net-like film. Vertically aligned Bi_2S_3 platelets were formed on the FTO substrate. Prolonging the reaction to 12 h, some region of the film was covered by flower-like microstructures (Fig. 3e). The magnified SEM shown in Fig. 3f revealed that the flowers were composed of sheets.

Furthermore, experiments with different temperatures were executed. Fig. 4a and b shows the SEM images of the product obtained at 120 °C for 8 h. The FTO substrate is covered with vertically aligned Bi_2S_3 platelets. It is noted that the side and the top surfaces of the platelets are very rough (Fig. 4a). Magnified SEM image shown in Fig. 4b presents that the top surface was composed of some tiny slices. When the temperature was increased to 190 °C, the FTO substrate is covered by uniform platelets with higher density compared with those of 160 °C. The platelets are thicker and stacked each other. The thicker sheets occupied more space between them, which might decrease the active area for photocatalytic degradation of organic compounds. This result indicates that 160 °C is the optimal reaction temperature for the formation of vertically aligned Bi_2S_3 platelets.

It is generally accepted that Tu can coordinate with metal ions to form metal-Tu complex, preventing the existence of large free metal ions and sulphur ions, and thus is favourable for the oriented growth of final product. Based on the structure and morphology prepared at different conditions, a possible formation mechanism of vertically aligned Bi_2S_3 platelets is proposed.

The growth rate of nuclei was slower because of the decomposition rate of the Bi—Tu complex ions. At the beginning of reaction, heterogeneous nucleation was much more preferential than

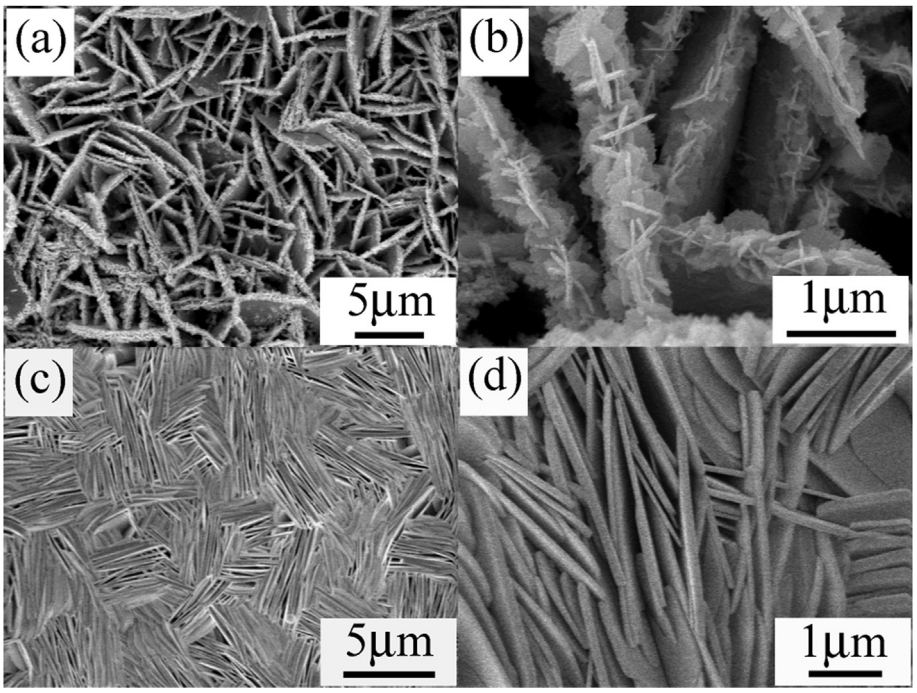

Fig. 4. SEM images of the products prepared at different temperatures: (a) and (b) 120 °C, (c) and (d) 190 °C.

the homogeneous nucleation due to the lower interfacial energy between substrate and solution, which resulted in the aggregation of nanoparticles on the FTO substrate [29]. With the consuming of the reactants, the process of the crystal growth continued and a layer of regimental petals composed of little nanosheets adhered to the substrate. Crystalline Bi_2S_3 belongs to the intrinsically anisotropic orthorhombic phase, and the crystal growth tends to obtain a match between the symmetry of the crystals and uniaxial geometry of one-dimensional species [31,32], which leads to the formation of little nanosheets. With the reaction time increasing, the building units of the precipitate on the substrate could grow larger into slices, which began to combine together and form vertically aligned Bi_2S_3 platelets.

The as-prepared vertically aligned Bi_2S_3 platelets have been tested for the applicability in photodegradating MB. Fig. 5a shows the absorption spectra of aqueous solution of MB in the presence vertically aligned Bi_2S_3 platelets irradiated by a UV lamp at different period of time. The intensity of the absorption peak corresponding to the MB molecules gradually decreases with the prolonging of the exposure time, and disappears completely at 240 min. To investigate the photocatalytic activity of vertically aligned Bi_2S_3 platelets, another two experiments were carried out: (i) Bi_2S_3 rods with the same area; (ii) adsorption experiments in darkness to examine whether the physisorption/chemisorption of vertically aligned Bi_2S_3 platelets plays important role on the fast decrease of the MB concentration. It could be observed that the absorption peak of the MB molecules still exists after 240 min exposure time for the Bi_2S_3 rods (Fig. 5b). For the adsorption experiments in darkness, very little MB is degraded. Because after being stirring in darkness for 240 min, the absorption peak corresponding to the MB molecules is still very strong (Fig. 5c).

The variations of MB concentration (C/C_0) with irradiation time are shown in Fig. 5d. It is found that the adsorption of MB was negligible without UV irradiation (less than 5% within 240 min). The addition of catalyst irradiated by the UV lamp leads to obvious degradation of MB. The comparative results shown in Fig. 5d also demonstrate that the degradation rate of MB for the vertically aligned Bi_2S_3 platelets [curve (1)] is higher than that for Bi_2S_3 rods [curve (2)]. A degradation ratio of 56% was obtained for the vertically aligned Bi_2S_3 platelets at 120 min and about 99% of the dye was degraded at 240 min. For the Bi_2S_3 rods, 42% MB was degraded after 120 min and 62% after 240 min. The photocatalytic activity of vertically aligned Bi_2S_3 platelets is also higher than that of Bi_2S_3 nanorods reported by Wu et al. For MB only about 40% degradation efficiency could be obtained at 120 min and less than 80% of the dye was degraded even after 240 min [17].

The reusabitlity and durability of the photocatalytic activity of the vertically aligned Bi_2S_3 platelets were also studied by reuse of the catalysts under the UV light irradiation, as shown in Fig. 6. After ten cycles of photodegradation process of MB, the loss of activity is not significant. It means the 2D nanostructure is very stable during the photocatalytic process.

Base on the traditional photocatalytic theory, the decomposition of the dye is believed to be initiated by the radicals of •OH and $O_2^{\cdot -}$. It is very important to avoid the recombination of the electron and hole for the continuous formation of •OH and $O_2^{\cdot -}$. Due to the small size of platelet, the photoinduced electron–hole pairs will diffuse to its surface rapidly and the recombination chance of electron–hole pairs inside the material will be largely reduced. More photogenerated electrons and holes can be used in photocatalytic reactions and MB can be degraded more rapidly. In addition, the larger specific surface area of vertically aligned Bi_2S_3 platelets is also beneficial to its excellent photocatalytic performance. Larger specific surface area will provide more active sites for the degradation reaction of organic compounds and effectively improve the separation efficiency of electron–hole pairs.

4. Conclusions

Vertically aligned Bi_2S_3 platelets on FTO substrate have been synthesized *via* simple hydrothermal process. It is found that the reaction time and temperature play key roles in driving the

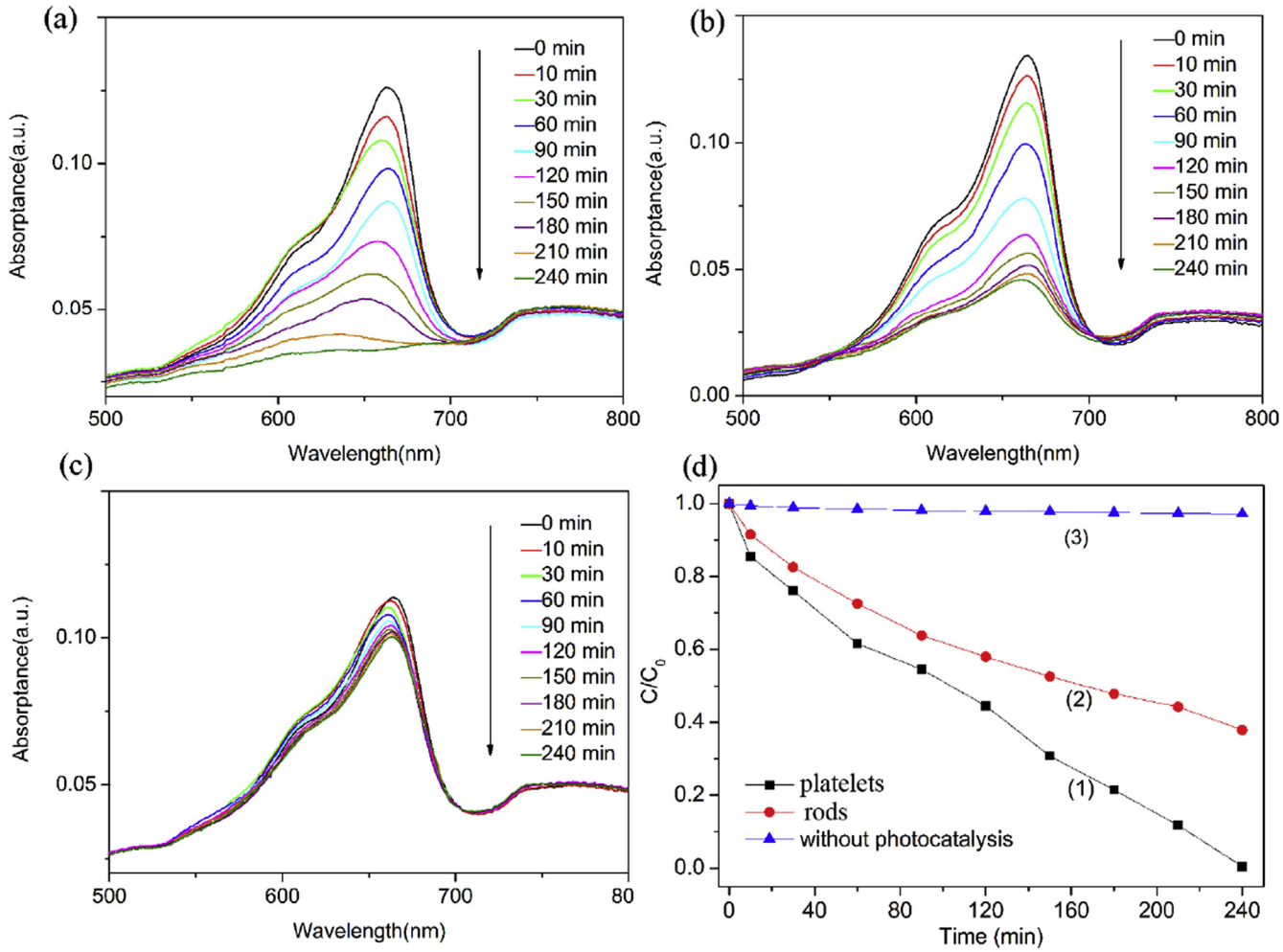

Fig. 5. Adsorption spectra of MB solutions in the presence of (a) vertically aligned Bi_2S_3 platelets, (b) Bi_2S_3 rods and (c) without UV irradiation, (d) photodegradation efficiency of MB in the presence of curve (1) vertically aligned Bi_2S_3 platelets, curve (2) Bi_2S_3 rods, curve (3) without UV irradiation.

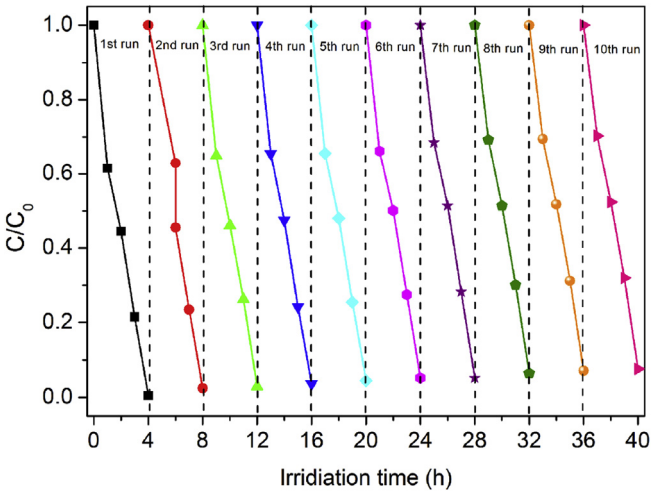

Fig. 6. Ten cycles of the photocatalytic reduction of MB using vertically aligned Bi_2S_3 platelets as the photocatalyst under UV irradiation for 240 min (4 h).

nucleation and the growth of vertically aligned Bi_2S_3 platelets. The Bi_2S_3 platelets exhibit excellent photocatalytic activity for degradation of MB under UV irradiation. It shows that Bi_2S_3 nanostructures have potential applications in the photocatalytic degradation of organic pollutants. The growth of Bi_2S_3 platelets on the substrate facilitates heterogeneous photocatalysis, which may be extended to the other catalysts.

Acknowledgement

This work was financially supported by the NSF of China (Grant No. 51302128), the NSF of Henan province (Grant Nos. 152300410114, 132300410085, 14B140009, 14B140008, 14A140018) and the program for Youth Scholar teachers Supporting Plan in Universities of Henan province (2013GGJS-189).

References

[1] G. Mor, O. Varghese, R. Wilke, S. Sharma, K. Shankar, T. Latempa, K. Choi, C. Grimes, p-Type Cu–Ti–O nanotube arrays and their use in self-biased heterojunction photoelectrochemical diodes for hydrogen generation, Nano Lett. 8 (2008) 1906–1911.
[2] Q. Zhang, L. Gao, J. Guo, Effects of calcination on the photocatalytic properties of nanosized TiO_2 powders prepared by $TiCl_4$ hydrolysis, Appl. Catal. B 26 (2000) 207–215.
[3] S. Khan, M. Al-Shahry, W.B. Ingler, Efficient photochemical water splitting by a chemically modified n-TiO_2, Science 297 (2002) 2243–2245.
[4] J.G. Yu, G.P. Dai, Q.J. Xiang, M. Jaroniec, Fabrication and enhanced visible-light photocatalytic activity of carbon self-doped TiO_2 sheets with exposed {001} facets, J. Mater. Chem. 21 (2011) 1049–1057.
[5] J.G. Yu, J. Zhang, A simple template-free approach to TiO_2 hollow spheres with

enhanced photocatalytic activity, Dalton Trans. 39 (2010) 5860–5867.
[6] A. Umar, M.S. Chauhan, S. Chauhan, R. Kumar, G. Kumar, S.A. Al-Sayari, S.W. Hwang, A. Al-Hajry, Large-scale synthesis of ZnO balls made of fluffy thin nanosheets by simple solution process: structural, optical and photocatalytic properties, J. Colloid Interface Sci. 363 (2011) 521–528.
[7] Q.J. Xiang, J.G. Yu, M. Jaroniec, Tunable photocatalytic selectivity of TiO_2 films consisted of flower-like microspheres with exposed {001} facets, Chem. Commun. 47 (2011) 4532–4534.
[8] S. Rengaraj, S. Venkataraj, C.W. Tai, Y.H. Kim, E. Repo, M. Sillanpää, Self-Assembled mesoporous hierarchical-like In_2S_3 hollow microspheres composed of nanofibers and nanosheets and their photocatalytic activity, Langmuir 27 (2011) 5534–5541.
[9] F.F. Dong, Y.M. Guo, J. Zhang, Y.H. Li, L. Yang, Q.L. Fang, H. Fang, K. Jiang, Size-controllable hydrothermal synthesis of ZnS nanospheres and the application in photocatalytic degradation of organic dyes, Mater. Lett. 97 (2013) 59–63.
[10] D.G. Chen, F. Huang, G.Q. Ren, D.S. Li, M. Zheng, Y.J. Wang, Z. Lin, ZnS nano-architectures: photocatalysis, deactivation and regeneration, Nanoscale 2 (2010) 2062–2064.
[11] L.Y. Mao, J.J. Li, Y.L. Xie, Y.J. Zhong, Y. Hu, Controllable growth of SnS_2/SnO_2 heterostructured nanoplates via a hydrothermal-assisted self-hydrolysis process and their visible-light-driven photocatalytic reduction of Cr(VI), RSC Adv. 4 (2014) 29698–29701.
[12] Y. Hu, X.H. Gao, L. Yu, Y.R. Wang, J.Q. Ning, S.J. Xu, X.W. Lou, Carbon-coated CdS petalous nanostructures with enhanced photostability and photocatalytic activity, Angew. Chem. Int. Ed. 52 (2013) 5636–5639.
[13] H. Zeynali, S.B. Mousavi, S.M. Hosseinpour-Mashkani, Synthesis and characterization of Bi/Bi_2S_3 nanocomposite through polyol method and its photovoltaic applications, Mater. Lett. 144 (2015) 65–68.
[14] J.F. Cabrita, V.C. Ferreira, O.C. Monteiro, Titanate nanofibers sensitized with nanocrystalline Bi_2S_3 as new electrocatalytic materials for ascorbic acid sensor applications, Electrochim. Acta 135 (2014) 121–127.
[15] M. Wang, Z.Q. Yang, Y.L. Guo, X.X. Wang, H.S. Yin, S.Y. Ai, Visible-light induced photoelectrochemical biosensor for the detection of microRNA based on Bi_2S_3 nanorods and streptavidin on an ITO electrode, Microchim. Acta 182 (2015) 241–248.
[16] Y.J. Lu, J.H. Jia, G.W. Yi, Selective growth and photoelectrochemical properties of Bi_2S_3 thin films on functionalized self-assembled monolayers, CrystEngComm 14 (2012) 3433–3440.
[17] T. Wu, X.G. Zhou, H. Zhang, X.H. Zhong, Bi_2S_3 nanostructures: a new photocatalyst, Nano Res. 3 (2010) 379–386.
[18] J. Zhou, G.H. Tian, Y.J. Chen, Y.H. Shi, C.G. Tian, K. Pan, H.G. Fu, Growth rate controlled synthesis of hierarchical Bi_2S_3/In_2S_3 core/shell microspheres with enhanced photocatalytic activity.
[19] E.L. Hu, X.H. Gao, A. Etogo, Y.L. Xie, Y.J. Zhong, Y. Hu, Controllable one-pot synthesis of various one-dimensional Bi_2S_3 nanostructures and their enhanced visible-light-driven photocatalytic reduction of Cr(VI), J. Alloys Compd. 611 (2014) 335–340.
[20] X.H. Gao, H.B. Wu, L.G. Zheng, Y.J. Zhong, Y. Hu, X.W. Lou, Formation of mesoporous heterostructured $BiVO_4/Bi_2S_3$ hollow discoids with enhanced photo-activity, Angew. Chem. Int. Ed. 53 (2014) 5917–5921.
[21] C.H. Wang, X.T. Zhang, Y.L. Zhang, Y. Jia, J.K. Yang, P.P. Sun, Y.C. Liu, Hydrothermal growth of layered titanate nanosheet arrays on titanium foil and their topotactic transformation to heterostructured TiO_2 photocatalysts, J. Phys. Chem. C 115 (2011) 22276–22285.
[22] Q.H. Mu, Q.H. Zhang, H.Z. Wang, Y.G. Li, Facile growth of vertically aligned BiOCl nanosheet arrays on conductive glass substrate with high photocatalytic properties, J. Mater. Chem. 22 (2012) 16851–16857.
[23] C.F. Guo, S.H. Cao, J.M. Zhang, H.Y. Tang, S.M. Guo, Y. Tian, Q. Liu, Topotactic transformations of superstructures: from thin films to two-dimensional networks to nested two-dimensional networks, J. Am. Chem. Soc. 133 (2011) 8211–8215.
[24] H. Zhang, J. Huang, X.G. Zhou, X.H. Zhong, Single-Crystal Bi_2S_3 nanosheets growing *via* attachment–recrystallization of nanorods, Inorg. Chem. 50 (2011) 7729–7734.
[25] Y. Zhao, Y. Xie, J.S. Jie, C.Y. Wu, S. Yan, Tectonic arrangement of Bi_2S_3 nanocrystals into 2D networks, J. Mater. Chem. 19 (2009) 3378–3383.
[26] J.M. Ma, Z.F. Liu, J.B. Lian, X.C. Duan, T. Kim, P. Peng, X.D. Liu, Q. Chen, G. Yao, W.J. Zheng, Ionic liquids-assisted synthesis and electrochemical properties of Bi_2S_3 nanostructures, CrystEngComm 13 (2011) 3072–3079.
[27] L. Li, N. Sun, Y. Huang, Y. Qin, N. Zhao, J. Gao, M. Li, H. Zhou, L. Qi, Topotactic transformation of single-crystalline precursor discs into disc-like Bi_2S_3 nanorod networks, Adv. Funct. Mater. 18 (2008) 1194–1201.
[28] C.J. Tang, Y.X. Zhang, X.C. Dou, G.H. Li, Seed-assistant hydrothermal synthesis of 3D Bi_2S_3 matlike architecture, J. Cryst. Growth 312 (2010) 692–697.
[29] S.J. Peng, P.N. Zhu, V. Thavasi, S.G. Mhaisalkara, S. Ramakrishna, Facile solution deposition of $ZnIn_2S_4$ nanosheet films on FTO substrates for photoelectric application, Nanoscale 3 (2011) 2602–2608.
[30] W. Zhao, T.Q. Lin, S.R. Sun, H. Bi, P. Chen, D.Y. Wan, F.Q. Huang, Oriented single-crystalline nickel sulfide nanorod arrays: “two-in-one” counter electrodes for dye-sensitized solar cells, J. Mater. Chem. A 1 (2013) 194–198.
[31] J. Tang, A.P. Alivisatos, Crystal splitting in the growth of Bi_2S_3, Nano Lett. 6 (2006) 2701–2706.
[32] B. Gates, Y.D. Yin, Y.N. Xia, A solution-phase approach to the synthesis of uniform nanowires of crystalline selenium with lateral dimensions in the range of 1030 nm, J. Am. Chem. Soc. 122 (2000) 12582–12583.